sustainability

MDPI

Article

Dynamic Modeling and Analysis of a Virtual Synchronous Generator with Supercapacitor

Meiling Ma *, Zhiyuan Zhi, Dong Han and Yushan Fan

School of Mechanical Engineering, University of Shanghai for Science and Technology, Shanghai 200093, China
* Correspondence: xhmml@126.com

Abstract: With the continuous integration of new energy sources, the power system gradually begins to present the characteristics of a weak power grid. The system's inertia decreases, leading to problems in the stability of the power grid. In this paper, a virtual synchronous generator model with a supercapacitor is analyzed. The supercapacitor provides additional virtual inertia to the system and suppresses system frequency disturbances more quickly. Bifurcation theory is used to analyze the nonlinear dynamics of the model. The bifurcation diagram of input active power is given in this paper, and the phase portraits and sequence diagrams of the frequency and power angle are presented to verify that, if the initial value of the system falls inside the stability region, the system can remain stable. If the initial value of the system falls outside the stability region, conversely, the system will lose stability. Finally, the simulation verifies the influence of the supercapacitor on the system inertia. The results show that the recovery speed of a small capacitance system is faster than that of a large capacitance system when disturbance occurs. It is concluded that, the smaller the supercapacitor is, the greater the virtual inertia it can provide.

Keywords: nonlinear dynamics; frequency stability; virtual synchronous generator; supercapacitor; bifurcation

Citation: Ma, M.; Zhi, Z.; Han, D.; Fan, Y. Dynamic Modeling and Analysis of a Virtual Synchronous Generator with Supercapacitor. *Sustainability* **2023**, *15*, 1248. https://doi.org/10.3390/su15021248

Academic Editor: Shuhua Fang

Received: 24 November 2022
Revised: 2 January 2023
Accepted: 6 January 2023
Published: 9 January 2023

1. Introduction

Renewable energy systems are developing rapidly, and intelligent and efficient converters need to be used to realize the various functions required by new power systems. The performance of the converter is directly related to the power quality. With the continuous integration of renewable energy systems with traditional power grids, a large number of nonlinear loads will be generated in the grids. Considering the long transportation lines of the distribution network, transformer leakage inductance, and other factors, the power grid presents weak grid characteristics [1,2]. Compared with conventional synchronous generators, renewable energy units based on droop control lack a dynamic frequency response and provide no support for the moment of inertia. With the continuous increase in renewable energy penetration, the system frequency stability will continue to decline. To solve the problem of the system inertia loss caused by droop control, some scholars have proposed virtual synchronous generator (VSG) control. Reference [3] proposes a control solution to realize the stable charging and discharging of the energy storage device by using a VSG, so that the direct current (DC) energy storage device can be stably connected to the AC (alternating current) microgrid and participate in grid frequency regulation. Reference [4] shows the value range of the VSG's virtual inertia and damping parameters under the constraint of its energy storage capacity and analyzed the influence of the energy storage charging and discharging power limit on the VSG's primary frequency modulation and performance. Reference [5] establishes the relationship between virtual inertia, virtual impedance, and energy storage capacity, and selects appropriate parameters to maintain the stability of the converter control system during power transmission. References [6–9] propose that, on the basis of a VSG, the system adaptively change the VSG parameters in

different response stages to obtain a better regulation effect and further exert the energy storage frequency support capability. The application of the VSG in nonlinear systems has gradually become a mature and effective control method.

Energy storage elements are required to maintain the stable, reliable, and efficient operation of the VSG. Reference [10] proposes a "bottom-up" energy management strategy based on multi-agent system. Each agent exchanges information through the communication network and determines its control mode by judging the status of its components (solar cells, batteries, etc.). It relies on communication links and sacrifices control speed and accuracy. Reference [11] proposes to manage the state of charge (SOC) of the battery by automatically adjusting the current of the fuel cell and providing or absorbing a certain amount of peak power by changing the current of the battery to maintain the stability of the DC bus voltage, obviously increasing the input cost. Based on the above considerations, supercapacitors (SC) can be used as energy storage devices. As an energy storage element with unique properties, a SC uses the electrolyte between its two solid conductors as the medium for energy storage. Therefore, it has a higher dielectric constant. In addition, its losses can be almost negligible, and its life is long. Compared with lead-acid batteries, which only have thousands of charge and discharge cycles, they can handle a large number of cycles and provide a higher current. SCs have many advantages and have been applied in many fields. For instance, they can be used as a backup power supply in electronic products such as memory, computers, timers, etc. They can also be used as the main power supply in electric toys, the starting power for internal combustion engines, and the auxiliary power supply for solar cells [12]. Some photovoltaic systems use SCs to smooth power fluctuations [13]. The development of SC has entered a mature period, and its commercial market is also growing. More companies will focus on the production of SCs [14].

Small-signal based stability analysis is a classical method. It evaluates the stability of the system by analyzing the distribution of eigenvalues related to the system state matrix in the complex plane. When the real part of all feature values is negative, the system is stable [15]. When the nonlinear process of the system leads to a large disturbance, the system has an instability risk. Although the research is still in the preliminary stage, it is still necessary to propose research on large signal modeling and stability analysis. Typical methods include the energy function method, bifurcation theory, graphic analysis, etc. [16]. Bifurcation theory plays an important role in the analysis of nonlinear systems. It has a high theoretical research value and practical application value [17]. When the dynamic parameter value exceeds the system's stability range, the system's behavior (such as the number of equilibrium points, periodic motion, and stability) will change suddenly, which often accompanied by chaos, fractals, mutation, etc. This phenomenon is called bifurcation [18]. There are many types of bifurcation, such as Hopf bifurcation, period-doubling bifurcation, etc. The essence of Hopf bifurcation is that the characteristic root of the Jacobian matrix of the system has a pair of conjugate pure imaginary solutions. The bifurcation diagram of period-doubling bifurcation has an obvious phenomenon of one splitting into two. In the modern power system, due to the extensive application of electrically powered devices and the use of various advanced nonlinear control systems, power systems have become increasingly complex high-dimensional nonlinear systems. Thus, the power system operates closer to the stability limit than before, and the operational uncertainty increases. Reference [19] studied the transient response of three-phase VSGs under the actual grid voltage drop and found the abrupt bifurcation phenomenon in the system. The converter shows irreversible instability after descending. An increase of the AC reactive current will have disastrous consequences for the system. The full-order eigenvalue analysis and the analysis method based on the reduced order mixed potential theory are used to reveal the physical origin of the large signal instability. The critical parameters of the system are identified, and the instability boundary of the system is determined. Reference [20] demonstrated a new instability scenario for grid voltage source converter limit-induced bifurcation (LIB) caused by the reference current limitation of the external control loop. When the current limit exceeds a certain critical value, the system may

immediately become unstable, and LIB may occur when meeting this limit. Bifurcation analysis is used to find the critical value of the dynamic parameters of the system, to facilitate the stability analysis of the nonlinear system and to determine the value range of the dynamic parameters.

According to the definition used in physics, inertia is an inherent attribute of an object that represents the ability of an object to resist the impact of an external force after being subjected to such an external force. Traditional power systems equipped with an SG have high inertia and damping and can therefore remain stable under small disturbances. Inertia can prevent a sudden change in the system frequency; that is, there is a kind of blocking effect. The size of a unit's inertia determines the size of the blocking effect of the unit on a sudden change in frequency [21]. Strong inertia can make the SG stabilize the system frequency under sufficient conditions and realize the active power balance. The existence of damping reduces the impact on the SG when a load is suddenly added and removed. When a frequency disturbance occurs in the system, the inertia hinders the frequency change and the damping suppresses the system oscillation. The two complements help each other to stabilize the grid. According to the current "source-grid-load-storage" power system structure, load-side and storage measurements can also provide potential inertia, so the integrated inertia of the current system is made up of the traditional SG inertia, load inertia, and virtual inertia [22].

The system inertia of a traditional SG is abundant. The inertia of a traditional SG in operation is represented by the amount of energy that hinders the rotation of the SG rotor. When a frequency disturbance occurs, the rotating kinetic energy of the SG rotor is released to provide inertia as support for the system. The other loads in the system also change their operating state and load power according to their own characteristics and frequency variations [23]. For new energy power systems, if the inertia simulation function is added to the system converter, the system can adjust its frequency with the converter [21–24]. At present, the control of the converter is mainly divided into two categories: the current tracking type and the voltage configuration. The current tracking type introduces the system frequency change rate in the active power control link and regulates the system power support through changes in the active power. The voltage configuration is to introduce the rotor motion equation and electromagnetic transient equation in the control link, and provide energy through the DC side system of the converter. These equations simulate similar characteristics of the SG. In this paper, the voltage configuration control method is used to simulate the rotor motion equation and realize the frequency regulation of the system.

The rest of this paper is organized as follows: Section 2 introduces the virtual synchronous generator model with a supercapacitor. Section 3 gives the bifurcation analysis of the proposed model. Section 4 sets simulation conditions to explore the effect of DC side capacitance on system frequency recovery. Section 5 summarizes this paper.

The contributions of this paper are as follows:

- Propose a SC-based VSG model for improving the frequency response speed.
- Calculate the stability region of the SC-based VSG model using bifurcation theory.

2. Nonlinear Dynamic Mathematical Model of the VSG with SC

2.1. VSG Control Strategy

The rotor motion equation of the traditional SG is the core idea of VSG control. In the mathematical model of the SG, the mechanical part is described by the rotor mechanical characteristic equation. Assuming that the mechanical loss is neglected, the corresponding equation is shown in (1). It can be seen from (1) that it mainly reflects the mechanical rotary inertia and damping characteristics of the synchronous generator rotor [25].

$$J_s\dot{\omega} = T_m - T_e - D_s\left(\omega - \omega_{ref}\right) \tag{1}$$

where $\omega - \omega_{ref}$ is the difference between the actual speed and the reference speed. T_m and T_e are the mechanical torque and electromagnetic torque of SG, J_s is the inertia of the SG, and D_s is the damping constant.

According to the governor and excitation regulation principle of the traditional SG, the VSG includes active frequency control and reactive voltage control. It also adds the moment of inertia and damping to enable it to display external characteristics similar to those of the traditional SG. The active frequency control of the VSG is shown in (2). Its principle is to change the output of the VSG by detecting the deviation of active power to achieve frequency regulation.

$$J_v\dot{\omega}_m = \frac{P - P_{ref}}{\omega_m} - D_v\left(\omega_m - \omega_{ref}\right) \tag{2}$$

where $P - P_{ref}$ is the difference between actual power and reference power, $\omega_m - \omega_{ref}$ is the difference between the actual speed and the reference speed. J_v is the virtual inertia; The damping constant D_v represents the adjustment degree of the frequency change to the active power, which makes the VSG show the inhibition effect on the oscillation. Compared with a synchronizer, the VSG shows a similar principle to that of the synchronizer. The difference between the mechanical power and electromagnetic power of the synchronizer corresponds to the difference between the actual power and reference power of the VSG. The speed difference of the synchronizer corresponds to the VSG's speed difference.

2.2. SC-Based VSG Modeling

The structural block diagram of the SC-based VSG is shown in Figure 1. The input power is defined as P_{in}, and the output power after passing through the DC side is P_{out}. A virtual impedance gain module Z(s) is added to provide the required impedance at the output. The output reference voltage from the virtual damping module and the reactive module minus the virtual impedance is divided by half of the DC side voltage (Vdc/2) to form the modulation index of the inverter switch [26]. The energy of the system is provided by the SC. The main reason for introducing the SC is that it can provide more than 10^5 charge and discharge processes, meaning that it has a better anti-aging effect than the traditional battery energy storage system. In addition, the SC has a faster response speed than traditional energy storage.

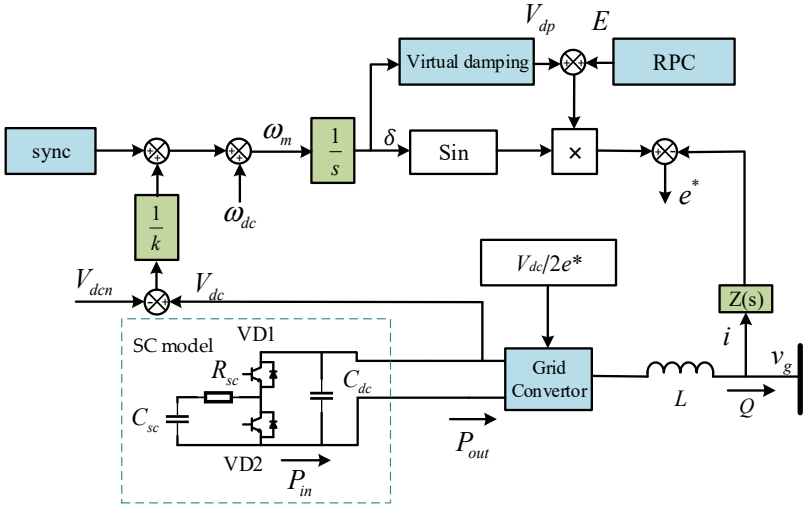

Figure 1. Virtual synchronous generator with supercapacitor modeling.

2.2.1. Virtual Damping

The damping part ($P_{dp} = D(\omega_g - \omega_m)$) in the SG should be added to the VSG. However, the point of application for P_{dp} is not available in the proposed controller. P_{dp}

has to be applied differently and is translated into voltage amplitude, namely V_{dp}, which is implemented at the output of the RPC block.

$$V_{dp} = -DV_g(\omega_g - \omega_m)\cos(\delta - \delta_g) \tag{3}$$

where V_g is the grid voltage, and δ_g is the power angle of the power grid. By adding the damping effect to the voltage amplitude, the simulation of the damping part of the VSG control is realized.

2.2.2. RPC

It can be seen from Figure 1 that the damping is introduced into the output voltage E. The reactive power control module adopts a voltage droop control, and the control block diagram is shown in Figure 2.

$$\begin{cases} Q_{ref} = Q_n - k_v(V_g - V_n) \\ \dot{E} = k_q\left(Q_{ref} - Q\right) \end{cases} \tag{4}$$

where Q_{ref} and Q_n are the reference value and real value of the reactive power in the system, respectively.

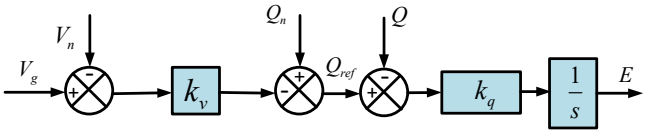

Figure 2. Reactive Power Control.

The voltage amplitude within the SG is proportional to the speed. However, droop control allows the voltage amplitude to be determined by the droop controller, and the dependence of voltage on speed is eliminated. This is why the internal voltage in the VSG proposed in this paper is not dependent on the speed, but is directly controlled through the RPC link.

2.2.3. SC Model

This paper adopts the classic energy storage model of the SC, namely the resistance capacitance (RC) model [13], as shown in Figure 1. The two triodes in the figure play a filtering role to ensure that the output terminal is DC voltage. According to Kirchhoff's voltage law, the mathematical model of the SC can be obtained:

$$U_{sc} = I_{sc}R_{sc} + \frac{1}{C_{sc}}\int I_{sc}dt \tag{5}$$

where U_{sc} is the output voltage of the SC. I_{sc} is the charge-discharge current of the SC, R_{sc} is the equivalent resistance, C_{sc} is the equivalent capacitance, and C_{dc} is the DC side capacitance of the system.

There are three cycle operation modes for SCs. In the first, the SC is kept in the constant DC charging mode until the terminal voltage of the SC is saturated, and then the terminal voltage is kept stable by discharging. This mode is called the energy storage mode. In the second, when the voltage provided by the power grid system is interrupted or dropped, the electric energy stored by the SC will supply power to the load through the DC converter. In this mode, which is called the constant voltage operation mode, the SC is in the discharge state. In the third, the SC does not operate; that is, there is no energy flow. This mode is called the standby holding mode.

The inertial energy of the VSG is obtained from the capacitance on the DC side of the converter. Part of the inertial energy can be directly supplied by the input source, if the time constant of the input source allows it. Assuming that the inertia required by the

system is J_t, the virtual inertia provided by the DC side capacitor of the converter $J = KC$, where the gain $K = kk_0$, the parameter k depends on the allowable swing range of the DC voltage, and the parameter k_0 depends on the rated value of the DC voltage V_{dcn}. In other words, to have the same inertia as the traditional SG, the required capacitance value needs to be determined as $C = J/K$ when setting the capacitance value.

In general, the inertia provided by the capacitor to the system is changed by changing the DC terminal voltage. This indicates that there is a relationship between the value of the capacitor and the inertia that can be provided to the system. Assuming that the inertia provided by the input terminal is J_{in}, the converter system equation can be further rewritten as

$$P_{in} - P_{out} = J_t \omega_m \dot{\omega}_m = J\omega_m \dot{\omega}_m + J_{in}\omega_m \dot{\omega}_m \tag{6}$$

The VSG system model with SC can be expressed in the form of the following set of equations containing six sets of state variables $(\omega_m, E, \delta, i_d, i_q, V_{dp})$, as shown in (7).

For each given active power input (P_{in}) and reactive power input (Q_n), the equilibrium point can be obtained by linearizing the nonlinear system model through the Jacobian matrix. Assume that the grid frequency and voltage are rated, i.e., $V_g = V_n$, $\omega_{m0} = \omega_g = \omega_{ref}$, $V_{dp0} = 0$, the equilibrium point of the system model becomes (ω_{m0}, E_0, δ_0, i_{d0}, i_{q0}, V_{dp0}) and the Jacobian matrix is given below.

The initial value of the output voltage is expressed as

$$E_0^2 = Y + V + \sqrt{(Y+V)^2 - Y^2 - \overline{Y}^2},\ Y = RP_{in} + L\omega_g Q_n,\ \overline{Y} = L\omega_g P_{in} - RQ_n,\ V = 0.5V_g^2$$

$$\begin{cases} \dot{\omega}_m = \frac{\int I_{sc}dt}{(U_{sc} - I_{sc}R_{sc})k} \frac{P_{in} - Ei_d - V_{dp}i_d}{V_{dcn} + k\left(\omega_m - \omega_{ref}\right)} \\ \dot{E} = k_q\left(Q_n + k_v\left(V_n - V_g\right) + Ei_q\right) \\ \dot{\delta} = \omega_g - \omega_m \\ \dot{i}_d = -\frac{R}{L}i_d + \frac{1}{L}\left(E + V_{dp}\right) - \frac{1}{L}v_{cd} + \omega_m i_q \\ \dot{i}_q = -\frac{R}{L}i_q - \frac{1}{L}v_{cq} - \omega_m i_d \\ \dot{V}_{dp} = -\frac{1}{\tau}V_{dp} - \frac{1}{\tau}DV_g\left(\omega_g - \omega_m\right)\cos\delta \end{cases} \tag{7}$$

$$\begin{bmatrix} 0 & \frac{-i_{d0}\times\int I_{sc}dt}{(U_{sc}-I_{sc}R_{sc})kV_{dcn}} & 0 & \frac{-E_0\times\int I_{sc}dt}{(U_{sc}-I_{sc}R_{sc})kV_{dcn}} & 0 & \frac{-i_{d0}\times\int I_{sc}dt}{(U_{sc}-I_{sc}R_{sc})kV_{dcn}} \\ 0 & k_q i_{q0} & 0 & 0 & k_q E_0 & 0 \\ -1 & 0 & 0 & 0 & 0 & 0 \\ i_{q0} & \frac{1}{L} & 0 & -\frac{R}{L} & \omega_{m0} & -\frac{1}{L} \\ -i_{d0} & 0 & 0 & -\omega_{m0} & -\frac{R}{L} & 0 \\ \frac{D}{\tau}V_g\cos\delta_0 & 0 & 0 & 0 & 0 & -\frac{1}{\tau} \end{bmatrix}$$

3. Bifurcation Analysis

In this section, bifurcation theory is adopted to analyze the nonlinear dynamics of the power angle and damping voltage. The initial condition of the system is set as $y_0 = [377, 828, 0.054, 5.5, -0.9, 0]$. Some of the system parameters are given in Table 1.

Table 1. Parameters of the VSC.

Parameter	Symbol	Value
DC side voltage rating	V_{dcn}	430 V
DC side capacitor	C_{dc}	880 μF
Damping constant	D	0.05
Grid frequency	f	60 Hz
Power factor	$\cos\varphi$	0.68

The bifurcation diagram for the active power P_{in} is shown in Figure 3. The solution changes suddenly at $P_{in} = 470.74$ W, which implies that the system bifurcates at that point.

When $P_{in} \leq 470.7$ W, the power angle converges to $\delta = -1$ after a short oscillation. This indicates that the system is stable. When $P_{in} \geq 470.8$ W, it can be seen in the Figure 3 that the power angle value starts to drop, which indicates that the system becomes unstable.

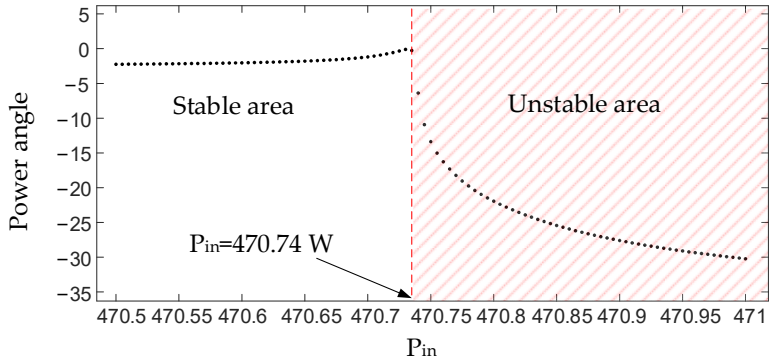

Figure 3. Bifurcation diagram.

Figure 4a,b are the phase portraits of $\delta - \omega_m$ and $V_{dp} - \omega_m$. When $P_{in} = 470.7$ W, the trajectory in Figure 4a approaches the stable equilibrium point eventually. When $P_{in} = 470.8$ W, the trajectory is attracted by the saddle point and separated from the stable equilibrium point gradually. The blue line in Figure 4b is the trajectory on the phase plane $V_{dp} - \omega_m$, when $P_{in} = 470.7$ W. It can be seen that the trajectory slowly converges to the stable equilibrium point. When $P_{in} = 470.8$ W, the trajectory ultimately breaks away from the stable equilibrium point, which implies that the system becomes unstable.

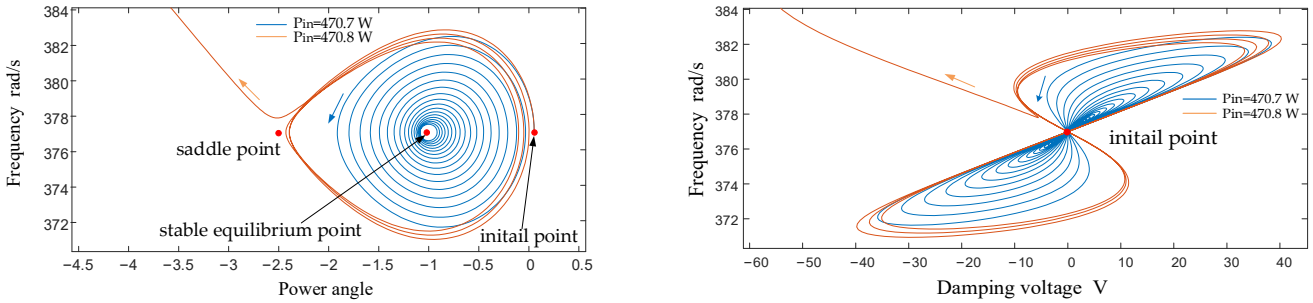

(**a**) $\delta - \omega_m$ (**b**) $V_{dp} - \omega_m$

Figure 4. Phase portraits of frequency-power angle and frequency-damping voltage.

Figure 5a,b are sequence diagrams of the power angle. When $P_{in} = 470.7$ W, the power angle approaches the equilibrium point $\delta_0 = -1$. When $P_{in} = 470.8$ W, the power angle breaks away from the stable equilibrium point, which corresponds to the sequence diagram, in which it starts to vibrate and then falls.

Figure 5c corresponds to the voltage sequence diagram when $P_{in} = 470.7$ W, and Figure 5d corresponds to the voltage sequence diagram when $P_{in} = 470.8$ W. When $P_{in} = 470.7$ W, the voltage value converges to the stable value 0 and finally tends to a steady state, as shown in Figure 5c. While $P_{in} = 470.8$ W, the voltage value starts to diverge and oscillate continuously after t = 1 s. The sequence diagrams of the power angle and voltage coincide with the stability intervals in the bifurcation diagram in Figure 3 and phase portraits in Figure 4.

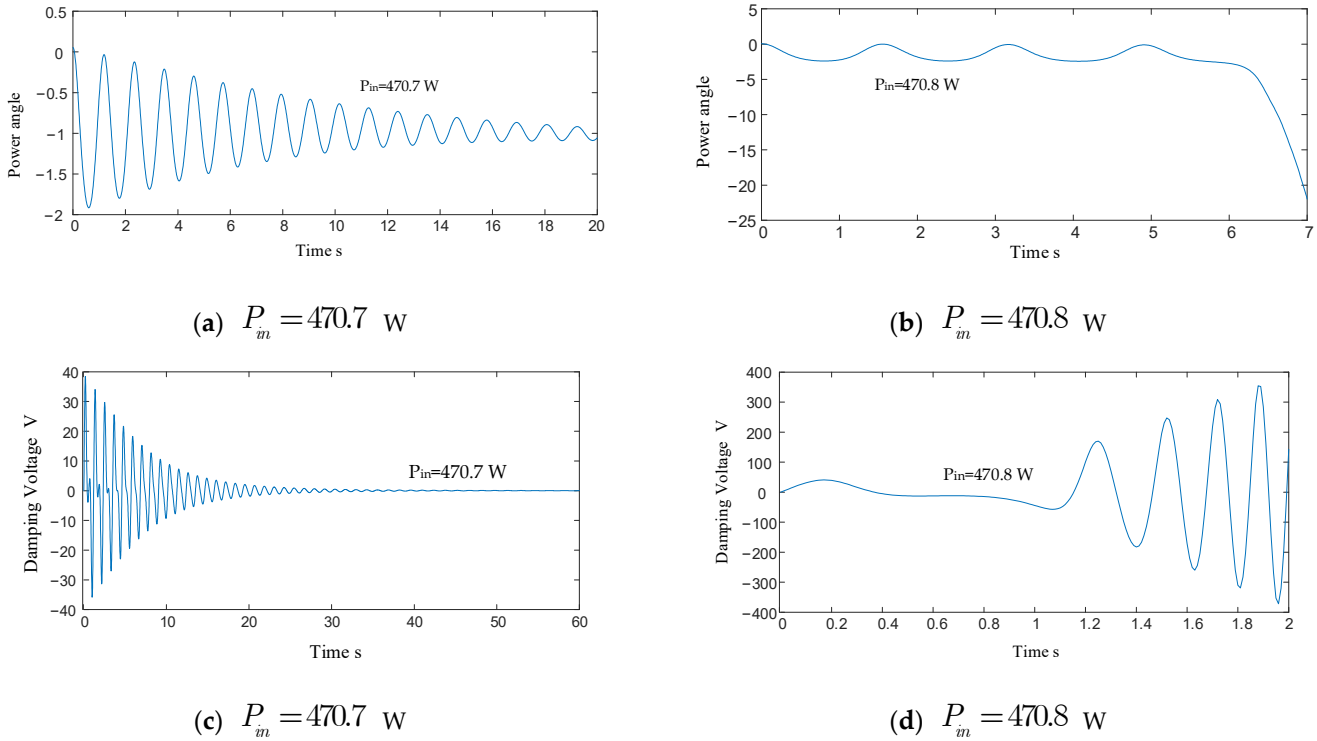

(**a**) $P_{in} = 470.7$ W (**b**) $P_{in} = 470.8$ W

(**c**) $P_{in} = 470.7$ W (**d**) $P_{in} = 470.8$ W

Figure 5. Sequence diagrams of power angle and damping voltage.

The structure and initial point of the system will change when the disturbance occurs in the system. If the initial value of the system falls inside the stability region, the system can remain stable through oscillation; that is, it has a certain anti-interference ability. If the initial value of the system falls outside the stability region, the system will lose stability.

4. Simulation

To verify the model proposed previously, this paper uses MATLAB/Simulink software to simulate and verify whether the system can inhibit the frequency disturbance and the extent to which the supercapacitance can inhibit the frequency disturbance of the system. Some simulation parameters are shown in Table 2:

Table 2. System Parameters.

Parameters	Symbols	Value
DC side voltage rating	V_{dcn}	430 V
DC side capacitor	C_{dc}	750 μF
Grid voltage	V_g	169.71 V
Grid frequency	f	60 Hz
Active power	P_{in}	142.65 W
Reactive power	Q_n	0.01 Var

A group of initial points in the system is set as (377.1, 0.0055, −4.56, −5.28, −1.81, −24.60). To simplify the simulation, the SC operates in the constant voltage mode after the system is disturbed. To verify the effect of the model on the frequency disturbance of the power grid, the proposed model is simulated in the following scenarios:

1. 0 s < t < 5 s, the system starts and operates normally;
2. 5 s < t < 8 s, the system frequency drops 0.1 Hz;
3. 8 s < t < 11 s, the system frequency rises 0.1 Hz;
4. 11 s < t < 14 s, the system adds 255 W active power and 255 Var reactive power;
5. 14 s < t < 17 s, the system reduces 100 W active power.

The simulation results are shown in Figure 6, where Figure 6a is the partial simulation diagram of the system with a frequency of falling and rising, and Figure 6b is the partial simulation diagram of the system with inrush and power reduction. It can be observed from Figure 6 that the controller can stably respond to the transient disturbance of the power grid, and, on this basis, it is stable at a new working point. This is because, when the input power jumps, the controller adjusts the power output so that the system frequency will maintain the current steady-state value. When active and reactive power is added to the system, the controller can also act quickly and restore the unit frequency to stability as soon as possible.

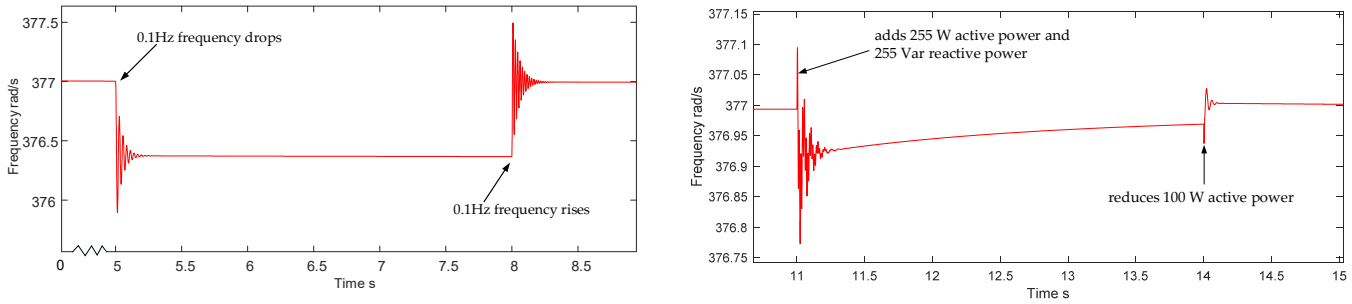

(**a**) (**b**)

Figure 6. System Frequency Simulation Diagram.

To verify that VSG control with a supercapacitor has a faster corresponding speed, the system with and without a supercapacitor is simulated and compared under the same conditions. When t = 5 s, the system has a 0.1 Hz frequency drop, and the result is shown in Figure 7. It can be seen from Figure 7 that the system with a supercapacitor can quickly reach the stability value after a frequency drop. The system without a supercapacitor can also recover to the stability value, but its recovery speed is not as fast as that of the other system. This is because the discharge speed of the supercapacitor is faster, and it can quickly transfer energy to the system in case of disturbance.

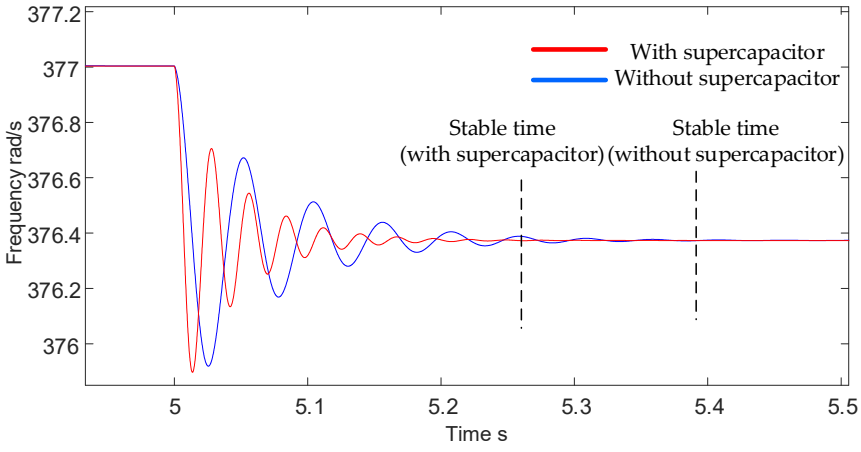

Figure 7. Comparison between supercapacitor and non-supercapacitor under frequency disturbance.

To verify the influence of the supercapacitor of the converter on the system inertia, a simulation experiment is carried out by changing the capacitance value to observe the regulating effect of different capacitance sizes on the system frequency in cases of disturbance. The variation range of the capacitance value is between 740 μF and 1.55 mF under the parameters of Table 2, which is verified by bifurcation analysis. The simulation results are shown in Figures 8 and 9. The red line capacitance value in Figure 8 is still 750 μF. The blue line capacitance is 950 μF. The green line capacitance is 1.5 mF. It can be

seen from Figure 8a that, after the system frequency drops 0.1 Hz at t = 5 s, capacitors of various capacities can well maintain the system frequency at a certain value. However, if the capacitance value is larger, the system recovery speed will be slower, and the inertia provided by the supercapacitor will be smaller. Figure 8b shows the results when the system frequency rises at t = 8 s. The system frequency change after the system's inrush of reactive and active power is shown in Figure 9. It can be seen from the Figure 9 that the smaller the capacitance value is at t = 11.02 s, the easier it is to suppress the frequency change and the faster the frequency stabilizes.

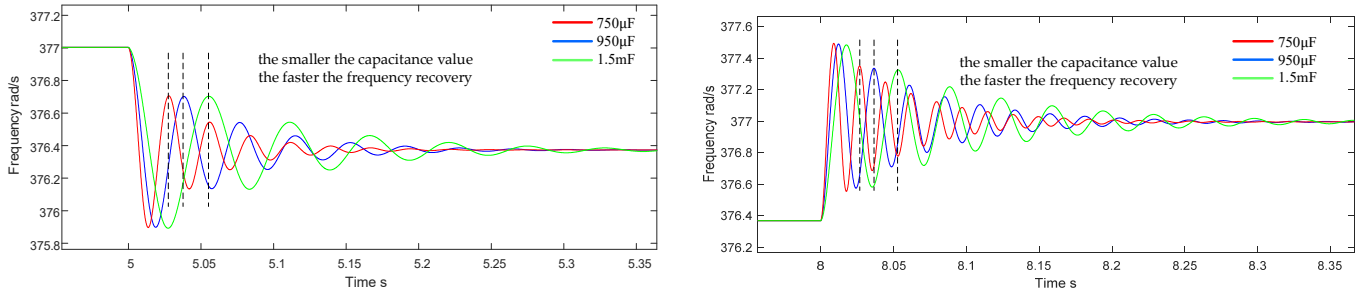

Figure 8. Frequency curves at frequency changes of three capacitors.

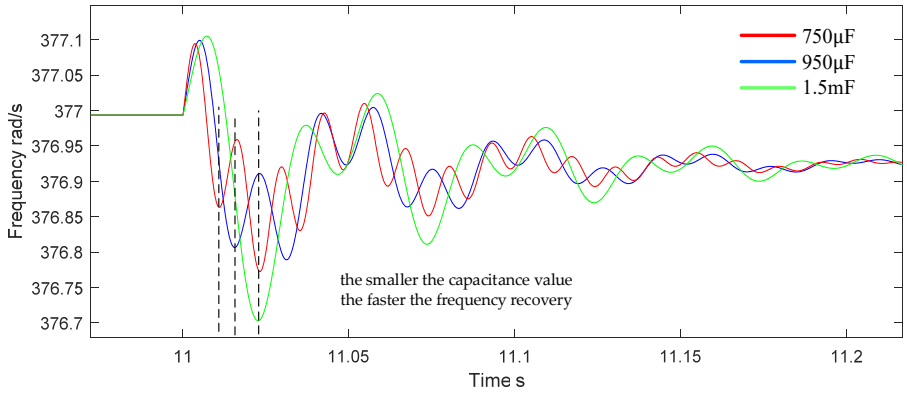

Figure 9. Frequency curve of inrush active power and reactive power in the system.

5. Conclusions

This paper studies the characteristic of the SC-based VSG model, which provides DC voltage to the system with its excellent energy storage advantage. The system uses the supercapacitor to provide virtual inertia to suppress frequency disturbances in the system. Bifurcation diagrams are presented to illustrate the dynamics of the system. The results show that the supercapacitor in the system can provide virtual inertia to the grid, and the magnitude of the virtual inertia is related to the supercapacitance. The smaller the supercapacitance, the faster the system recovers after a frequency disturbance, which also proves that the smaller supercapacitor can provide more virtual inertia to the system. The inadequacy of this study is that, when the system frequency is disturbed due to a sudden influx of active and reactive power in the power grid, the system cannot highlight the faster response speed caused by the change of capacitance. How to quickly restrain the inflow and outflow of power is the focus of the next stage of our research.

Author Contributions: Conceptualization, Z.Z.; Methodology, M.M.; Software, M.M.; Formal analysis, M.M. and Z.Z.; Investigation, Z.Z.; Resources, M.M.; Data curation, Y.F.; Writing—original draft, Z.Z.; Writing—review & editing, Z.Z. and Y.F.; Visualization, Y.F.; Supervision, D.H. All authors have read and agreed to the published version of the manuscript.

Funding: This research was funded by Shanghai Sailing Program grant number (22YF1429500).

Institutional Review Board Statement: The study did not require ethical approval.

Informed Consent Statement: The study did not involve humans.

Data Availability Statement: We decided not to share the research data.

Conflicts of Interest: The authors declare no conflict of interest.

References

1. Xie, L.; Zeng, S.; Liu, J.; Zhang, Z.; Yao, J. Control and Stability Analysis of the LCL-Type Grid-Connected Converter without Phase-Locked Loop under Weak Grid Conditions. *Electronics* **2022**, *11*, 3322. [CrossRef]
2. Xie, L.; Huang, J.; Tan, E.; He, F.; Liu, Z. The Stability Criterion and Stability Analysis of Three-Phase Grid-Connected Rectifier System Based on Gerschgorin Circle Theorem. *Electronics* **2022**, *11*, 3270. [CrossRef]
3. Gao, F.; Wang, X.; Yang, P.; Kou, S.; Sun, M. Research and Simulation of Hybrid AC/DC Microgrid. In Proceedings of the 2020 4th International Conference on HVDC (HVDC), Xi'an, China, 6–9 November 2020; pp. 1276–1280.
4. Mao, M.; Hu, J.; Chang, L. Power Distribution Strategy & Real-time Simulation for VSG-controlled Parallel PV/Battery Microgrid Using RT-LAB. In Proceedings of the 2019 IEEE 10th International Symposium on Power Electronics for Distributed Generation Systems (PEDG), Xi'an, China, 3–6 June 2019; pp. 919–924.
5. Li, S.; Gao, S.; Guo, C. Multi-objective optimal capacity allocation of hybrid energy storage. *J. Power Supply* **2018**, *16*, 174–180. (In Chinese)
6. Li, D.; Zhu, Q.; Lin, S.; Bian, X.Y. A self-adaptive inertia and damping combination control of VSG to support frequency stability. *IEEE Trans. Energy Convers.* **2016**, *32*, 397–398. [CrossRef]
7. Zhang, X.; Mao, F.; Xu, H.; Liu, F.; Li, M. An optimal coordination control strategy of micro-grid inverter and energy storage based on variable virtual inertia and damping of VSG. *Chin. J. Electr. Eng.* **2017**, *3*, 25–33.
8. Li, X.; Chen, G. Improved Adaptive Inertia Control of VSG for Low Frequency Oscillation Suppression. In Proceedings of the 2018 IEEE International Power Electronics and Application Conference and Exposition (PEAC), Shenzhen, China, 4–7 November 2018; pp. 1–5.
9. Liu, J.; Yang, D.; Yao, W.; Fang, R.; Zhao, H.; Wang, B. PV-based virtual synchronous generator with variable inertia to enhance power system transient stability utilizing the energy storage system. *Prot. Control Mod. Power Syst.* **2017**, *2*, 429–437. [CrossRef]
10. Lagorse, J.; Paire, D.; Miraoui, A. A multi-agent system for energy management of distributed power sources. *Renew. Energy* **2010**, *35*, 174–182. [CrossRef]
11. Khaligh, A.; Rahimi, A.M.; Lee, Y.J.; Cao, J.; Emadi, A.; Andrews, S.D.; Robinson, C.; Finnerty, C. Digital control of an isolated active hybrid fuel cell/Li-ion battery power supply. *IEEE Trans. Veh. Technol.* **2007**, *5*, 3709–3721. [CrossRef]
12. Hu, C.C.; Chang, K.H.; Lin, M.C.; Wu, Y.T. Design and Tailoring of the Nanotubular Arrayed Architecture of Hydrous RuO2 for Next Generation Supercapacitors. *Nano Lett.* **2006**, *6*, 2690–2692. [CrossRef]
13. ŞahİN, M.E.; Blaabjerg, F.; SangwongwanİCh, A. Modelling of supercapacitors based on simplified equivalent circuit. *CPSS Trans. Power Electron. Appl.* **2021**, *6*, 31–39. [CrossRef]
14. Hu, C.C.; Chen, W.C.; Chang, K.H. How to Achieve Maximum Utilization of Hydrous Ruthenium Oxide for Supercapacitor. *J. Electrochem. Soc.* **2004**, *151*, A281–A282. [CrossRef]
15. Wang, X.; Taul, M.G.; Wu, H.; Liao, Y.; Blaabjerg, F.; Harnefors, L. Grid-Synchronization Stability of Converter-Based Resources—An Overview. *IEEE Open J. Ind. Appl.* **2020**, *1*, 115–134. [CrossRef]
16. Xiong, L.; Liu, X.; Liu, Y.; Zhuo, F. Modeling and stability issues of voltage-source converter dominated power systems: A review. *CSEE J. Power Energy Syst.* **2015**, *8*, 1530–1549.
17. Lazaros, L.; Christos, V.; Ioannis, S. Antimonotonicity, Hysteresis and Coexisting Attractors in a Shinriki Circuit with a Physical Memristor as a Nonlinear Resistor. *Electronics* **2022**, *11*, 1920.
18. Xia, J.; Mi, X. Bifurcation Analysis for Power System Voltage Stability Based on Singular Perturbation Method. In Proceedings of the 2007 International Conference on Electrical Machines and Systems (ICEMS), Seoul, Republic of Korea, 8–11 October 2007; pp. 1811–1814.
19. Huang, M.; Peng, Y.; Tse, C.K.; Liu, Y.; Sun, J.; Zha, X. Bifurcation and Large-Signal Stability Analysis of Three-Phase Voltage Source Converter Under Grid Voltage Dips. *IEEE Trans. Power Electron.* **2017**, *32*, 8868–8879. [CrossRef]
20. Xing, G.; Min, Y.; Chen, L.; Mao, H. Limit Induced Bifurcation of Grid-Connected VSC Caused by Current Limit. *IEEE Trans. Power Syst.* **2021**, *36*, 2717–2720. [CrossRef]
21. Ma, J.; Qiu, Y.; Li, Y.; Zhang, W.; Song, Z.; Thorp, J.S. Research on the Impact of DFIG Virtual Inertia Control on Power System Small-Signal Stability Considering the Phase-Locked Loop. *IEEE Trans. Power Syst.* **2017**, *32*, 2094–2105. [CrossRef]
22. Schiffer, J.; Aristidou, P.; Ortega, R. Online Estimation of Power System Inertia Using Dynamic Regressor Extension and Mixing. *IEEE Trans. Power Syst.* **2019**, *34*, 4993–5001. [CrossRef]
23. Best, R.J.; Brogan, P.V.; Morrow, D.J. Power System Inertia Estimation Using HVDC Power Perturbations. *IEEE Trans. Power Syst.* **2021**, *36*, 1890–1899. [CrossRef]

24. Wang, X.; Ding, L.; Ma, Z.; Azizipanah-Abarghooee, R.; Terzija, V. Perturbation-Based Sensitivity Analysis of Slow Coherency with Variable Power System Inertia. *IEEE Trans. Power Syst.* **2021**, *36*, 1121–1129. [CrossRef]
25. Shi, K.; Song, W.; Ge, H.; Xu, P.; Yang, Y.; Blaabjerg, F. Transient Analysis of Microgrids with Parallel Synchronous Generators and Virtual Synchronous Generators. *IEEE Trans. Energy Convers.* **2020**, *35*, 95–105. [CrossRef]
26. Khajehoddin, S.A.; Karimi-Ghartemani, M.; Ebrahimi, M. Grid-Supporting Inverters with Improved Dynamics. *IEEE Trans. Ind. Electron.* **2019**, *66*, 3655–3667. [CrossRef]